Stellar Masses and Star Formation Histories for 80,000 Galaxies from the Sloan Digital Sky Survey

Guinevere Kauffmann[1], Timothy M. Heckman[2], Simon D.M. White[1] , Stéphane Charlot[1,3], Christy Tremonti[2], Eric W. Peng[2], Mark Seibert[2], Mariangela Bernardi[4], Jon Brinkmann[5], Francisco J. Castander[6], Istvan Csábai[7,2], Masataka Fukugita[8], Zeljko Ivezic[9], Jeffrey A. Munn [10], Robert C. Nichol[11], Aniruddha R. Thakar[2], David H. Weinberg[12]

[1] *Max-Planck Institut für Astrophysik, D-85748 Garching, Germany*
[2] *Department of Physics and Astronomy, Johns Hopkins University, Baltimore, MD 21218*
[3] *Institut d'Astrophysique du CNRS, 98 bis Boulevard Arago, F-75014 Paris, France*
[4] *Department of Astronomy, University of Chicago, 5640 South Ellis Ave, Chicago, IL 60637*
[5] *Apache Point Observatory, P.O. Box 59, Sunspot, NM 88349*
[6] *Department of Physics, Yale University, P.O. Box 208121, New Haven, CT 06520*
[7] *Department of Physics, Eotvos Lorand University, Pf. 32, H-1518 Budapest, Hungary*
[8] *Institute for Cosmic Ray Research, University of Tokyo, Chiba 277-8582, Japan*
[9] *Princeton University Observatory, Peyton Hall, Princeton NJ 08544-1001*
[10] *US Naval Observatory, Flagstaff Station, P.O. Box 1149, Flagstaff, AZ 86002*
[11] *Department of Physics, Carnegie Mellon University, 5000 Forbes Ave, Pittsburgh, PA 15232*
[12] *Department of Astronomy, Ohio State University, 140 West 18th Avenue, Columbus, OH 43210*

Abstract

We develop a new method to constrain the star formation histories, dust attenuation and stellar masses of galaxies. It is based on two stellar absorption line indices, the 4000 Å break strength and the Balmer absorption line index $H\delta_A$. Together, these indices allow us to constrain the mean stellar ages of galaxies and the fractional stellar mass formed in bursts over the past few Gyr. A comparison with broad band photometry then yields estimates of dust attenuation and of stellar mass. We generate a large library of Monte Carlo realizations of different star formation histories, including starbursts of varying strength and a range of metallicities. We use this library to generate median likelihood estimates of burst mass fractions, dust attenuation strengths, stellar masses and stellar mass-to-light ratios for a sample of 80,000 galaxies drawn from the Sloan Digital Sky Survey. The typical 95% confidence range in our estimated stellar masses is $\pm$ 40 %. We study how the stellar mass-to-light ratios of galaxies vary as a function of absolute magnitude, concentration index and photometric pass-band and how dust attenuation varies as a function of absolute magnitude and 4000 Å break strength. We also calculate how the total stellar mass of the present Universe is distributed over galaxies as a function of their mass, size, concentration, colour, burst mass fraction and surface mass density.

Keywords: galaxies:formation,evolution; galaxies: stellar content

1 Introduction

The masses of galaxies are traditionally estimated by dynamical methods from the kinematics of their stars and gas. From the time extended HI rotation curves were first measured for spirals, it has been clear that the implied masses include not only the observed material, but also substantial amounts of dark matter. Indeed, it is now believed that most galaxies are surrounded by dark halos which extend to many times their optical radii and contain an order of magnitude more mass than the visible components. The properties of these halos can be inferred directly from tracers at large radii such as X-ray emitting atmospheres, systems of satellite galaxies, or weak gravitational distortion of background galaxy images. In practice, gaseous atmospheres are visible only around some bright elliptical galaxies, while the other two techniques are too noisy to apply to individual galaxies; they are used to obtain average halo properties for stacked samples of similar galaxies (Zaritsky et al 1993 ; McKay et al 2002).

In order to understand how galaxies formed, we would like to map the relationship between the properties of the observed baryonic components of galaxies and those of their dark halos. This mapping should yield information about how the baryons cooled, condensed and turned into stars as the halo-galaxy systems were assembled, and should clarify the complex physical processes that regulated the efficiency and timing of galaxy formation.

Most studies of the halo-galaxy relation have used luminosity as a surrogate for total baryon content, and a kinematic measure – peak rotation velocity, stellar velocity dispersion, X-ray atmosphere temperature – as a surrogate for halo mass. Both surrogates are far from ideal. Kinematic measures are strongly affected by the visible components of the galaxy and so have an uncertain relation to halo mass; only satellite and weak lensing studies can reliably estimate total halo masses, albeit as an average over all galaxies in a chosen class. Galaxy luminosity may not correlate well with stellar mass (the dominant baryonic component in all but a subset of the smallest systems). There are strong dependences on the fraction of young stars in the galaxy and on its dust content. Thus a technique to correct for attenuation by dust and to estimate the mass-to-light ratio of the underlying stellar population is needed to estimate the stellar mass of a galaxy.

It is well-known that luminosities are less affected by stellar population variations in the near-infrared than in the optical and that extinction corrections are also smaller at longer wavelengths. Recently Verheijen (2001) studied the B, R, I and K'-band Tully-Fisher relations of a volume-limited sample of 49 spiral galaxies in the Ursa Major Cluster. He showed that the K'-band relation exhibited the tightest correlation with rotation velocity, suggesting that the stellar masses of galaxies are linked closely with the masses of the dark matter halos in which they formed. The larger scatter in the shorter wavelength passbands was attributed to variations in star formation history and dust extinction between different galaxies in the sample.

Although near-infrared luminosities are less dependent on star formation history than optical luminosities, they nevertheless exhibit some sensitivity to stellar age. Bell & de Jong

(2001) estimate that the near-infrared mass-to-light ratios of local spirals can vary by as much as a factor of two and propose a correction based on the optical colours of the galaxies. Brinchmann & Ellis (2000) also used colour-based methods to transform the near-infrared magnitudes of a sample of intermediate redshift galaxies into stellar masses. In both analyses, it was assumed that the star formation histories of galaxies could be described by simple exponential laws. If galaxies formed a major ($> 10\%$) fraction of their stars in recent bursts, it was shown that this would introduce substantial errors into the estimated mass-to-light ratios.

In this paper, we make use of spectral indicators as diagnostics of the past star formation histories of galaxies. In particular, two spectral features, the 4000 Å break and the Hδ absorption line, provide important information about the ages of the stellar populations in galaxies and are able to distinguish recent star formation histories dominated by bursts from those that are more continuous. We develop a method based on these two indicators and on broad-band photometry that allows us to derive maximum likelihood estimates of the stellar mass of a galaxy, the attenuation of its starlight by dust, and the fraction of its stars formed in recent bursts. We apply our method to a sample of $\sim 80,000$ galaxies drawn from the Sloan Digital Sky Survey and show how the derived stellar mass-to-light ratios of galaxies in four Sloan bandpasses (g, r, i and z; Fukugita et al 1996) depend both on galaxy luminosity and on structural parameters such as concentration index. We also compute the fraction of the total stellar mass in the Universe in galaxies of different masses, sizes, colours and concentrations. The dependence of galaxy properties on stellar mass is addressed in a separate paper (Kauffmann et al 2002; Paper II)

2 The Observational Sample

The sample of galaxies analyzed in this paper is drawn from the Sloan Digital Sky Survey. This survey will obtain u, g, r, i and z photometry of almost a quarter of the sky and spectra of at least 700,000 objects. The survey goals and procedures are outlined in York et al. (2000) and a description of the data products and pipelines is given in Stoughton et al.(2002).

Our sample of galaxies is is drawn from all available spectroscopic observations taken prior to MJD 52078. This data represents roughly 10% of the projected survey total. It only includes objects that are classified as galaxies by the Spectro1d pipeline (v5.3.3). Details of the spectroscopic target selection of galaxies are given in Strauss et al (2002). We have included all galaxies with Petrosian r band magnitudes in the range $15.5 < r^* < 17.7$ after correction for foreground galactic extinction using the reddening maps of Schlegel, Finkbeiner & Davis (1998) (Note that since the photometric calibration is still preliminary, we affix an asterisk to the filter when referring to SDSS camera magnitudes). This is slightly shallower than the 'main' galaxy sample designed for large-scale structure studies, which extends to a limiting r band magnitude of 17.77. Our sample contains a total of 81,429 galaxies. More details about the SDSS photometric system may be found in Fukugita et al (1996) and Smith

et al (2002). Information relating to the SDSS camera and photometric monitoring system can be found in Gunn et al (1998) and Hogg et al (2001).

The spectra were reduced using version v4.8.1 of the Spectro2d pipeline. The spectral indicators (primarily the 4000 Å break and the $H\delta_A$ index) and the emission lines (the equivalent widths and fluxes of $H\alpha$ and $H\beta$) that are discussed in this manuscript are calculated using a special-purpose code written by Christy Tremonti and Mark Seibert. A detailed description of the code is given in Tremonti et al (2002). A major feature of this code is its handling of Balmer lines. For a large percentage of emission line galaxies, the underlying Balmer stellar absorption is very strong. The code attempts to account for this by performing a simultaneous absorption plus emission line fit to each of the Balmer lines.

All magnitudes quoted in this paper are Petrosian magnitudes. For the SDSS, the Petrosian radius is defined as the largest radius at which the local r-band surface brightness is at least one fifth the mean surface brightness interior to that radius. The Petrosian flux is then the total flux within a circular aperture two times the Petrosian radius. Details about the Petrosian flux measurements are given in Lupton et al (2002) and Strauss et al (2002). The SDSS Petrosian magnitude detects essentially all the light from galaxies with exponential profiles and more than 80% of the light from galaxies with de Vaucouleurs profiles.

Conversions from apparent magnitude to absolute magnitude depend on cosmology through the distance modulus DM(z) and on galaxy type through the K-correction K(z):

$$M = m - DM(z) - K(z). \tag{1}$$

We assume a Friedman-Robertson-Walker cosmology with $\Omega = 0.3$, $\Lambda = 0.7$ and H_0= 70 km s $^{-1}$ Mpc^{-1}. We have used the most recent version of the Bruzual & Charlot (1993) models to generate lookup tables of K-corrections to the rest-frame g, r, i and z-band magnitudes of galaxies based on their observed $g - r$, $r - i$ and $i - z$ colours and on redshift. We do not attempt to K-correct the u-band magnitudes of the galaxies in our sample, because procedures based on the local slope of the spectral energy distribution have been shown to yield unreliable results (Blanton, private communication).

3 Spectral Diagnostics of Bursts

The break occurring at 4000 Å is the strongest discontinuity in the optical spectrum of a galaxy and arises because of the accumulation of a large number of spectral lines in a narrow wavelength region. The main contribution to the opacity comes from ionized metals. In hot stars, the elements are multiply ionized and the opacity decreases, so the 4000 Å break will be small for young stellar populations and large for old, metal-rich galaxies. A break index D(4000) was defined by Bruzual (1983) as the ratio of the average flux density F_ν in the bands 4050-4250 Å and 3750-3950 Å. A definition using narrower continuum bands (3850-3950 Å and 4000-4100 Å) was recently introduced by Balogh et al (1999). The principle advantage of the narrow definition is that the index is considerably less sensitive to reddening effects.

We will adopt the narrow definition as our standard in this paper and we denote this index as $D_n(4000)$. The evolution of $D_n(4000)$ following an instantaneous burst of star formation is illustrated in the top left panel of Fig. 1. The red line illustrates the result for solar metallicity, while the blue line is for a 20% solar model. As can be seen, the evolution of $D_n(4000)$ does not depend strongly on metallicity until ages of more than 10^9 years after the burst.

Strong Hδ absorption lines arise in galaxies that have experienced a burst of star formation that ended $\sim 0.1 - 1$ Gyr ago. The peak occurs once hot O and B stars, which have weak intrinsic absorption, have terminated their evolution, and the optical light from the galaxies is dominated by late-B to early-F stars. The current Bruzual & Charlot models have a 20 Å spectral resolution – too low to measure the Hδ absorption feature reliably. Worthey & Ottaviani (1997) have defined an Hδ_A index using a central bandpass bracketed by two pseudo-continuum bandpasses and have parametrized the strength of this feature as a function of stellar effective temperature, gravity and metallicity using the Lick/IDS spectral library, which has a spectral resolution of 9 Å. The index strengths in galaxies may then be computed by weighting the contributions from individual stars by their level of continuum. The evolution of the Hδ_A index following an instantaneous burst is shown in the top right panel of Fig.1 for solar and 20% solar metallicity models.

Although the evolution of the $D_n(4000)$ and Hδ_A indices does depend on metallicity, particularly at late times, it can be shown that the *locus* of galaxies in the $D_n(4000)$/Hδ_A plane is not sensitive to metallicity (or to extinction) and is a powerful diagnostic of whether galaxies have been forming stars continuously or in bursts over the past 1-2 Gyr. This is illustrated in the bottom two panels of Fig. 1, where we plot Hδ_A as a function of $D_n(4000)$ for a "pure burst" star formation history (left) and for continuous star formation histories (right) spanning a large range of ages (1.5-14 Gyr) and star formation timescales . As can be seen, the continuous models occupy a narrow band in the $D_n(4000)$/Hδ_A plane. Galaxies with stronger Hδ_A absorption strength at a given value of $D_n(4000)$ must have formed some fraction of their stars in a recent burst.

In Fig 2. we show the region of the $D_n(4000)$/Hδ_A plane populated by SDSS galaxies. We show the subset of galaxies for which the error in the measured value of Hδ_A is less than 1.2 Å and the error in the $D_n(4000)$ index is less than ~ 0.03. This cut includes ∼21,007 galaxies or 25% of the total sample. We have corrected the Hδ_A measurements for contamination due to nebular emission. Because the Hδ emission is so much weaker than that at Hα or Hβ, even in the dust-free case, the most robust way to correct for it is to scale directly from the measured Hα equivalent width. We use the difference between the observed Hα/Hβ emission line fluxes and the dust-free case-B recombination value (2.86) to calculate the attenuation of the emission lines. We assume an attenuation law of the form $\tau_\lambda \propto \lambda^{-0.7}$ (Charlot & Fall 2000). It is then straightforward to calculate the emission correction to the $H\delta_A$ index. We apply this correction to all galaxies with $H\beta$ equivalent widths less than -1 Å(where negative values denote emission). Fig. 2 shows that there is on the whole excellent agreement between the area of the $D_n(4000)$/Hδ_A plane populated by real galaxies and the values predicted by the population synthesis models. There is a small offset of about 1 Å on the Hδ_A index between

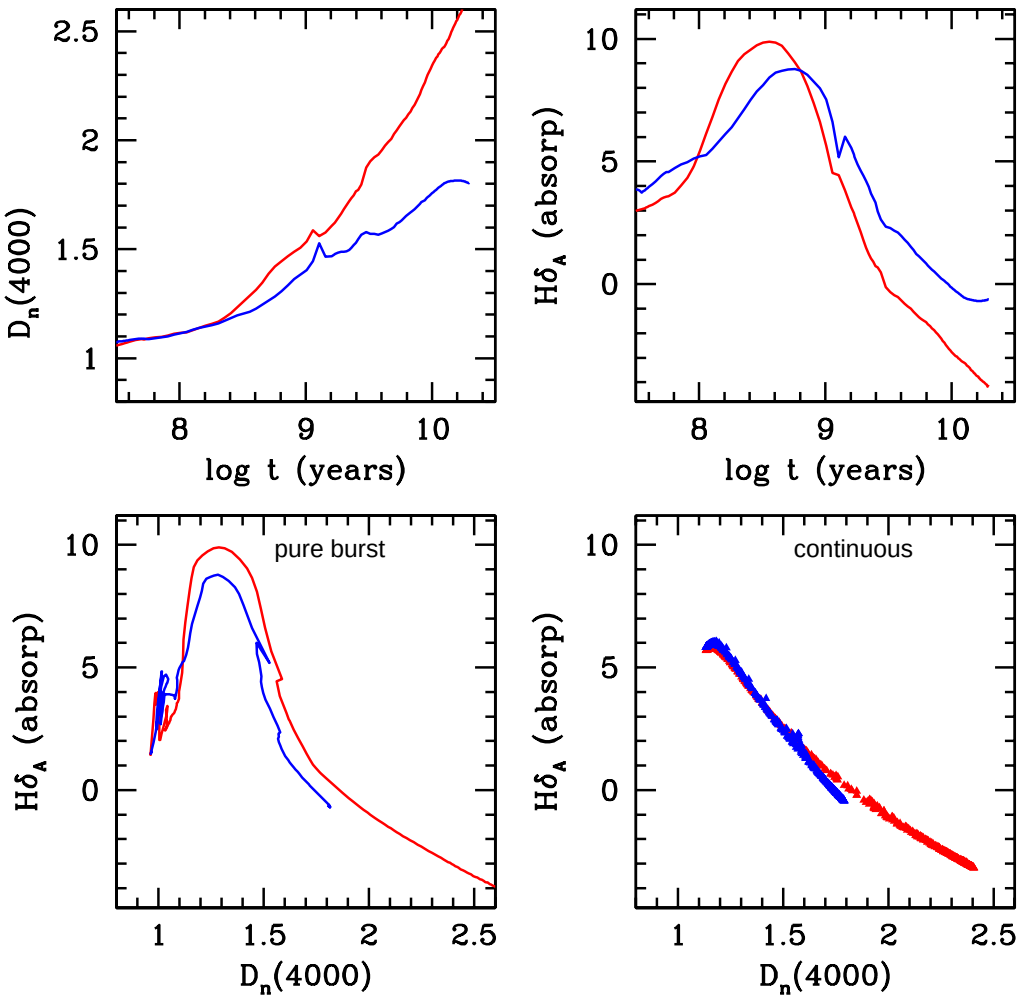

Figure 1: **Top:** The evolution of $D_n(4000)$ and $H\delta_A$ following an instantaneous burst of star formation. Red lines are for solar metallicity, blue lines are for 20% solar. **Bottom:** $H\delta_A$ is plotted as a function of $D_n(4000)$ for a pure burst model and for continuous models with a range of ages and star formation timescales. Once again, red is for solar models and blue is for 20% solar.

the models and the data at large values of $D_n(4000)$. Fig. 2 also shows that a substantial number of galaxies lie well away from the locus of continuous models and have thus undergone recent bursts of star formation. We now investigate the effect of bursts on the estimated stellar mass-to-light ratios of our galaxies.

4 A Library of Star Formation Histories

We have used a Bayesian technique to derive maximum likelihood estimates of the stellar mass-to-light ratios, dust attenuation corrections and burst mass fractions for each galaxy in our sample. We have also derived associated confidence intervals for each of these parameters. A generalized description of the mathematical basis of our technique is given in Appendix A.

In Bayesian statistics, an initial assumption is made that the data are randomly drawn from a distribution, which is a family of models characterized by a parameter vector $\mathbf{P}$. One has to specify a prior distribution on the space of all possible $\mathbf{P}$. This is a probability density distribution that encodes knowledge about the relative likelihood of various $\mathbf{P}$ values in the absence of any data. Typically one takes a uniform prior in parameters with a small dynamic range and a uniform prior in the logarithm of parameters with a large dynamic range.

We have set up our prior distribution by generating a library of Monte Carlo realizations of different star formation histories. It is important that our library of models span the full range of physically plausible star formation histories, and that it be uniform in the sense that all histories are reasonably represented and no a priori implausible corner of parameter space accounts for a large fraction of the models.

In our library, each star formation history consists of two parts:

1. An underlying continuous model parametrized by a formation time t_{form} and and a star formation time scale parameter γ. Galaxies form stars according to the law SFR(t) $\propto$ exp[$-\gamma t$(Gyr)] from time t_{form} to the present. We take t_{form} to be distributed uniformly over the interval from the Big Bang to 1.5 Gyr before the present day, and γ over the interval 0 to 1.

2. We have superimposed random bursts on these continuous models. The amplitude of a burst is parametrized as $A = M_{burst}/M_{cont}$, where M_{burst} is the mass of stars formed in the burst and M_{cont} is the total mass of stars formed by the continuous model from time t_{form} to the present. A is distributed logarithmically from 0.03 to 4.0. During the burst, stars form at a constant rate for a time t_{burst} distributed uniformly in the range 3×10^7 – 3×10^8 years. Bursts occur with equal probability at all times after t_{form} and we have set the probability so that 50% the galaxies in the library have experienced a burst in the past 2 Gyr. Our library is thus unbiased – bursting and continuous models are equally represented. (Recall that our stellar indicators $H\delta_A$ and $D_n(4000)$ are only sensitive to bursts occurring during the past 1-2 Gyr).

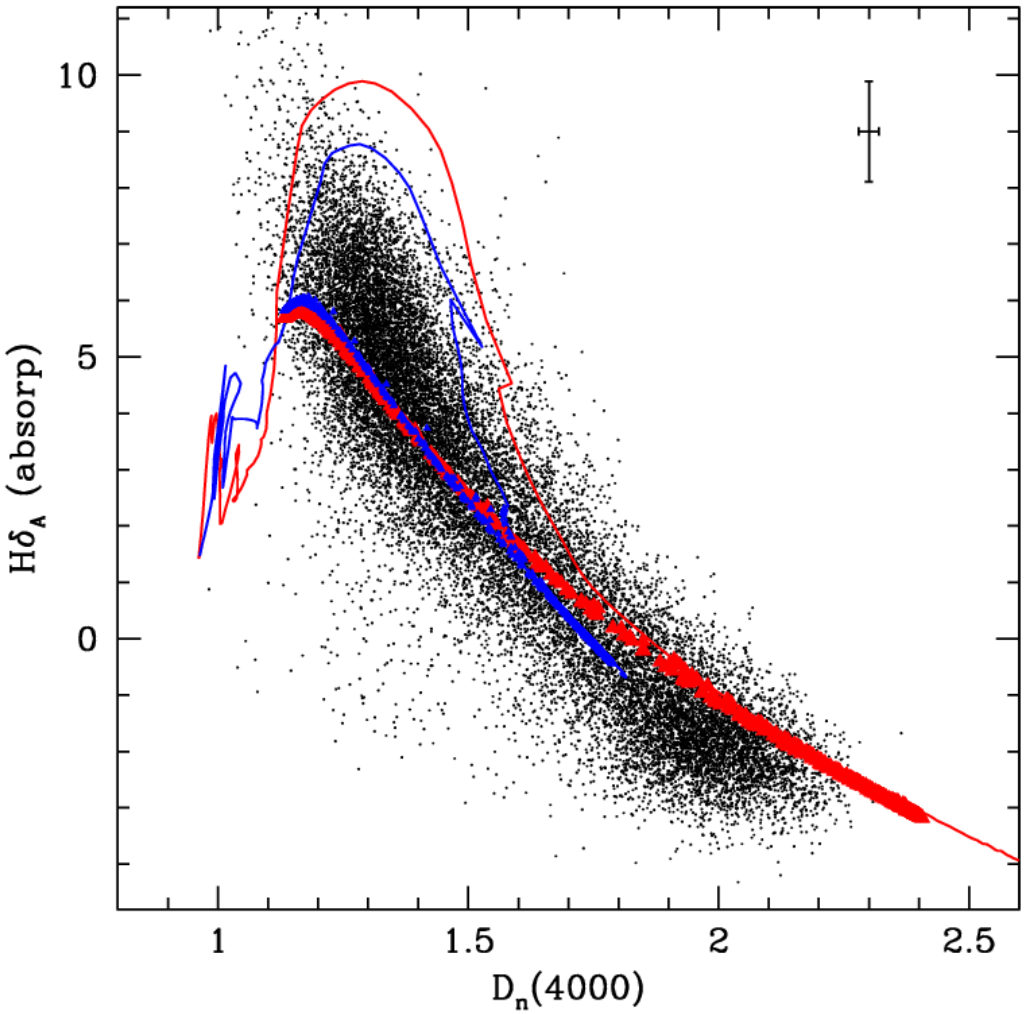

Figure 2: $H\delta_A$ is plotted as a function of $D_n(4000)$ for galaxies in the SDSS sample. The typical error bar on the indices is shown in the top right-hand corner of the plot. Red and blue lines and symbols indicate the regions of the diagram occupied by galaxies undergoing pure burst or continuous star formation, as explained in Fig 1.

We have adopted the universal initial mass function (IMF) as parametrized by Kroupa (2001). It is very similar in form to the IMF proposed by Kennicutt (1983). Our models are distributed uniformly in metallicity from 0.25 to 1.5 times solar. Our final library consists of 24,000 different star formation histories. For each history, we store a variety of different parameters, including the predicted values of $D_n(4000)$, $H\delta_A$, the value of the stellar mass-to-light ratio in the z-band, the $r-i$ colours of the stellar populations of the model galaxies, and the fraction of the total stellar mass of the galaxy formed in the burst mode in the past 2 Gyr (we will denote this parameter as F_{burst}). Fig. 3 illustrates how our model galaxies populate the $D_n(4000)/H\delta_A$ plane. Even though 50% of galaxies have had a starburst of varying amplitude in the past 2 Gyr, most of the models lie close to the locus of continuous star formation histories. The fact that our models are distributed inhomogeneously in the $D_n(4000)/H\delta_A$ plane has significant impact on the confidence intervals we derive for our parameters. For example, a galaxy will have a relatively high probability of being scattered from the continuous to the bursting region of the plane by observational errors. It will have a much smaller probability of being scattered the other way around. We will illustrate this in more detail in the next section.

In the left-hand panel of Fig. 4, we have divided the $D_n(4000)/H\delta_A$ plane into bins and we have colour-coded each bin to reflect the average z-band mass-to-light ratio of the stellar populations of the simulated galaxies that fall into it. As can be seen, the mass-to-light ratio is is primarily a sequence in $D_n(4000)$, but at fixed $D_n(4000)$, galaxies with strong $H\delta$ absorption have a higher fraction of young stars and hence have smaller mass-to-light ratios. As well as average values, one can also compute the 1σ dispersion in these parameters as a function of position in the plane. This is shown in the right hand panel of Fig. 4 and gives an indication of the accuracy with which mass-to-light ratios could be derived from the models if there were no observational errors and in the absence of dust. As can be seen, the logarithm of the z-band mass-to-light ratio can be determined to better than 0.1 dex for galaxies with $D_n(4000) > 1.7$. For galaxies with $D_n(4000) < 1.7$, $\log\,(M/L)_z$ is still determined to better than 0.15 dex for all but the very youngest systems.

In Fig. 5, the bins are colour-coded according to the average value of F_{burst}, the fraction of the stellar mass of the galaxy that formed in bursts over the past 2 Gyr. The right-hand panel of Fig. 5 shows the the distribution of $\sigma(F_{burst})/F_{burst}$. The burst mass fractions are only determined to better than 50% for galaxies with very strong $H\delta$ absorption.

5 Parameter Estimation from the Data

In this section, we apply our method to our sample of SDSS galaxies to estimate parameters such as burst mass fractions, stellar masses and dust attenuations. For each galaxy in the sample, we have a measurement of $D_n(4000)$ and $H\delta_A$ as well as an estimate of the error in these measurements. The likelihood that a galaxy has a given value of a parameter is evaluated by weighting each model in the library by the probability function $\exp(-\chi^2/2)$ and

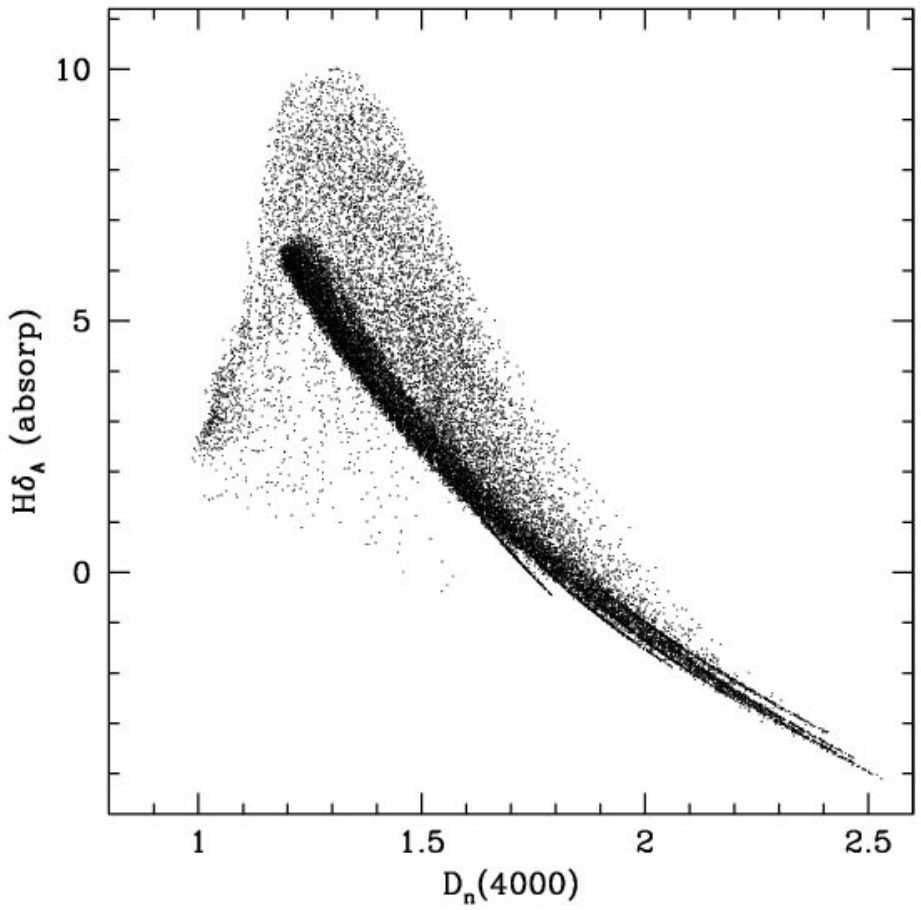

Figure 3: The distribution of galaxies in our model library in the $D_n(4000)/H\delta_A$ plane.

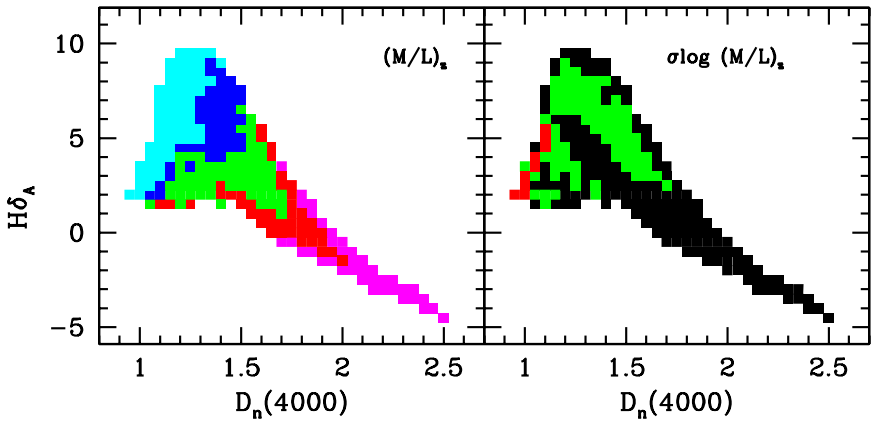

Figure 4: *Left:* The $D_n(4000)/H\delta_A$ plane has been binned and colour-coded to reflect the average z-band mass-to-light ratios of the simulated stellar populations that fall into that bin. Magenta indicates regions with $\log(M/L)_z > 0.15$, red is for $0 < \log(M/L)_z < 0.15$, green is for $-0.15 < \log(M/L)_z < 0$, blue is for $-0.3 < \log(M/L)_, z < -0.15$ and cyan is for $\log(M/L)_z < -0.3$. *Right:* The plane has been binned and colour-coded to reflect the 1σ dispersion in the z-band mass-to-light ratios. Black indicates regions with $\sigma \log(M/L)_z < 0.1$, green is for $0.1 < \sigma \log(M/L)_z < 0.15$ and red is for $\sigma \log(M/L)_z > 0.15$.

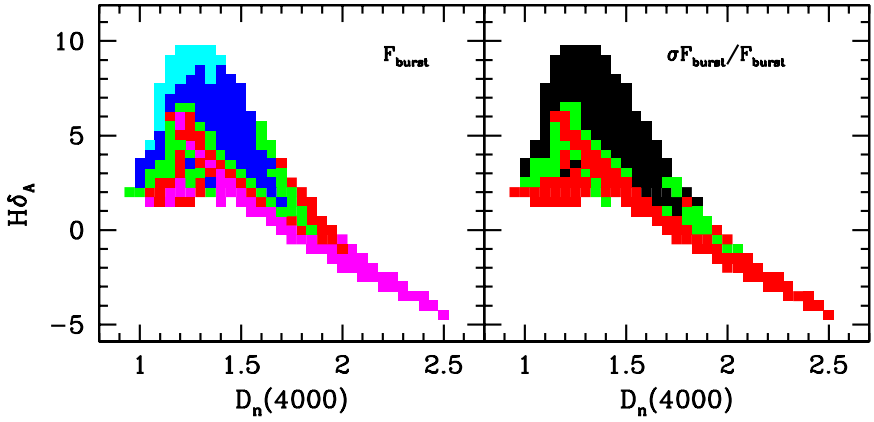

Figure 5: As in Fig. 4, except for the parameter F_{burst}. In the left panel, magenta is for $F_{burst} < 0.03$, red is for $0.03 < F_{burst} < 0.1$, green is for $0.1 < F_{burst} < 0.25$, blue is for $0.25 < F_{burst} < 0.5$ and cyan is for $F_{burst} > 0.5$. In the right panel, black is for $\sigma(F_{burst})/F_{burst} < 0.50$, green is for $0.5 < \sigma(F_{burst})/F_{burst} < 1.0$, and red is for $\sigma(F_{burst})/F_{burst} > 1.0$.

then binning the probabilities as a function of the parameter value (see Appendix A). The most likely value of the parameter can be taken as the peak of this distribution; the most typical value is its median. We define the 95% confidence interval by excluding the 2.5% tails at each end of the distribution.

5.1 Recovering $D_n(4000)$ and $H\delta_A$: a simple test of the method

It is informative to compare the *estimated* values of $D_n(4000)$ and $H\delta_A$ with the *observed* values of the same parameters. From now on, we will use the median value of the derived probability distributions as our "best" estimate of these parameters (in practice, the peak and the median usually give similar answers). The results of this comparison are shown in Fig. 6. The method recovers the observed value of $D_n(4000)$ to well within the 1σ observational error. However, $H\delta_A$ is not recovered as accurately. There are two reasons for this. The first reason is that the models are homogeneously distributed in $D_n(4000)$, but heterogeneously distributed in $H\delta_A$ (see Fig. 3). As a result, models with $H\delta_A$ far away from the observed value often contribute significantly to the probability distribution. This is why the distribution of differences between $H\delta_A$(estimated) and and $H\delta_A$(observed) shown in Fig. 6 is broad compared to the same distribution derived for the $D_n(4000)$ index. The second reason is that the data is offset from the models at large values of $D_n(4000)$ (see Fig. 2). This is why the $H\delta_A$ difference distribution is skewed towards negative values.

Fig. 7 compares the 2.5 and 97.5 percentile ranges of the estimated values of $D_n(4000)$ and $H\delta_A$ with the observational errorbars. We note that the observational errors on the $D_n(4000)$ index are very small – typically around 0.02 or a few percent of the total range of values spanned by the models. On the other hand, the $H\delta_A$ index has a typical error of 1-2 Å, which is more than 10% of the range spanned by the models. As can be seen from Fig. 7, the 2.5 and 97.5 percentile ranges of the probability distribution of $D_n(4000)$ correspond extremely well to the 2σ observational errors. However, the same is not true for $H\delta_A$. Because the error bars on this index are large, the range of acceptable $H\delta_A$ values is strongly constrained by the region of parameter space occupied by the models. As a result, 2.5 and 97.5 percentile values are typically less than 2σ away from the best estimate. We stress that these effects are due to genuine *physical constraints*, caused by the fact that $H\delta_A$ can only extend over a limited range of values for all possible star formation histories.

5.2 Estimating Burst Mass Fractions

Fig. 8 shows the probability distributions of the parameter F_{burst} that we derive for three galaxies drawn from our observational sample.

The top galaxy lies in the region of $D_n(4000)/H\delta_A$ parameter space occupied by galaxies that have formed stars continuously over the past few Gyr. This is reflected in the derived probability distribution, which is sharply peaked at a value of $F_{burst} = 0$. There is a small tail towards non-zero values of F_{burst}, reflecting the fact that the galaxy could have had a small

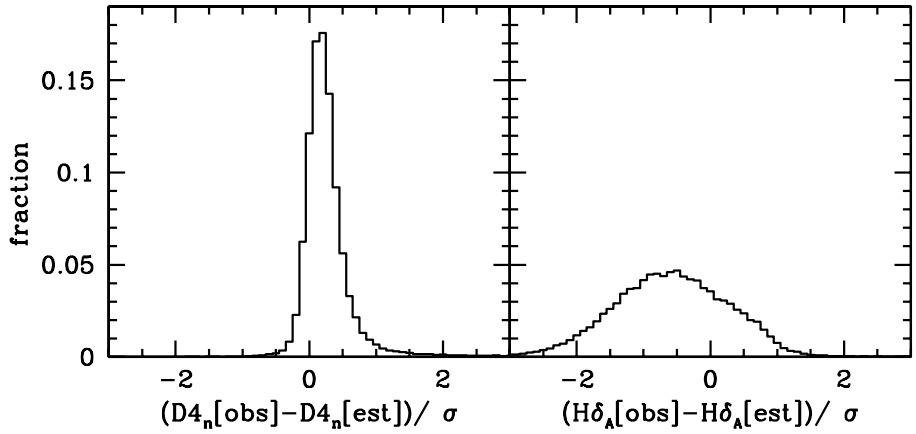

Figure 6: *Left:* The distribution of the observed value of $D_n(4000)$ minus the estimated one, divided by the 1σ measurement error for all galaxies in the SDSS sample. *Right:* The same thing except for the $H\delta_A$ index.

burst of star formation in the past that would not be detectable at the present day.

The middle galaxy lies well away from the locus of continuous star formation models. $D_n(4000)$ and $H\delta_A$ are both measured with high accuracy. As a result, our derived probability distribution indicates that this galaxy *must* have formed more than about 25% of its stars in a recent burst. The value of F_{burst} is not very well constrained. This reflects the so-called age/mass degeneracy: a large burst that occurred long ago is indistinguishable from a smaller burst that occurred more recently.

The bottom galaxy lies away from the locus of continuous models, but the error on its $H\delta_A$ index is much larger than that of the middle galaxy. The median value of the probability distribution indicates that a *typical* galaxy with the same $H\delta_A$ and $D_n(4000)$ index measurements will have experienced a burst during the past 2 Gyr. However, one cannot say with any degree of confidence that this particular galaxy must have undergone such a burst.

Our method thus provides us with an objective way of defining a sample of "post-starburst" galaxies from the data. We study the properties of such a sample in detail in Paper II.

5.3 Estimating the Attenuation of Starlight by Dust

So far, we have only calculated mass-to-light ratios and colours of the stellar populations of galaxies. We have not taken into account the attenuation of the starlight by dust in the interstellar medium. In the z-band, dust attentuation is not expected to be large, but it may nevertheless have substantial impact on our analysis of mass-to-light ratios, particularly if certain kinds of galaxies are much more dusty than others.

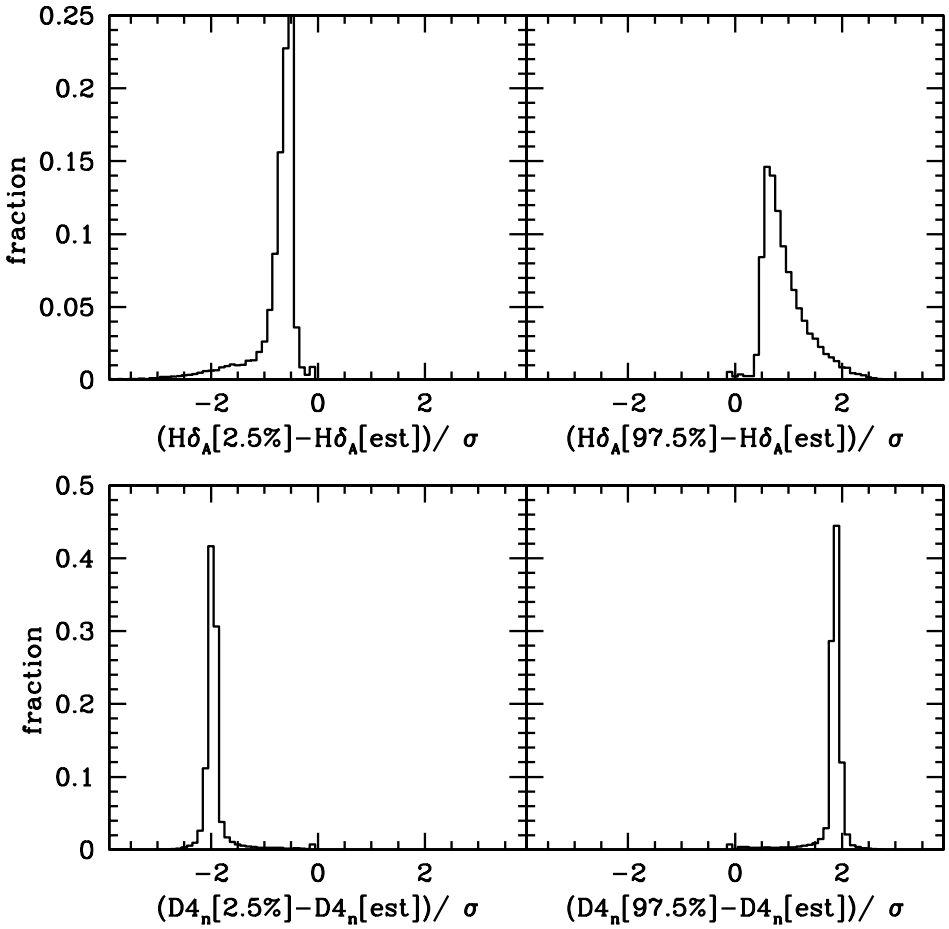

Figure 7: *Left:* The 2.5 percentile values of the probability distributions of $D_n(4000)$ and $H\delta_A$ minus the best estimates, divided by the 1σ measurement error. *Right:* The same thing except for the 97.5 percentile value. These histograms contain the data for our full SDSS sample.

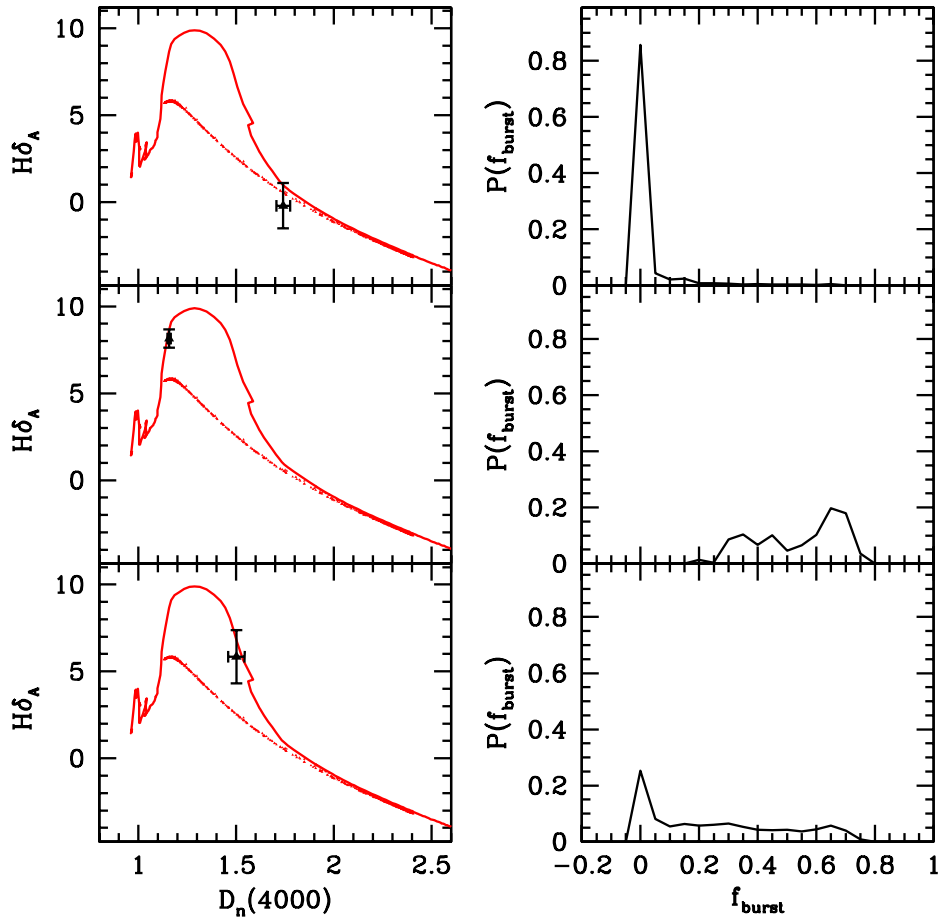

Figure 8: The left-hand panels show the location of three example galaxies in the $D_n(4000)/H\delta_A$ plane. Error bars indicate the measurement errors of the $D_n(4000)$ and $H\delta_A$ indices. The right-hand panels show the probability distributions of the parameter F_{burst} for each galaxy.

We can use our models to estimate the degree of dust attenuation by comparing our best estimate of the $r-i$ colour of the stars from our model library, to the observed colour of the galaxy. Note that we choose $r-i$ rather than $i-z$ because the photometric errors are smaller in the r and i bands than in the z band. In addition, the $r-i$ colour of a stellar population is sensitive primarily to its age, whereas at longer wavelengths the dependence of colours on metallicity becomes more important (Worthey 1994; Ferreras, Charlot & Silk 1999). This difference between the estimated colour and the observed colour allows us to calculate the reddening. By extrapolating to the z-band using a standard attenuation curve of the form $\tau_\lambda \propto \lambda^{-0.7}$, we obtain an estimate of A_z, the attenuation in the z-band expressed in magnitudes. We note that the shape of the attenuation curve determined from direct observations resembles a power law with slope ~ -0.7 over a wavelength range from 1250-8000 Å (Calzetti, Kinney & Storchi-Bergmann 1994). Models based on a 2-component ISM suggest that the extinction curve may be slightly steeper than this at longer wavelengths (Charlot & Fall 2000), but we will use a single power-law for simplicity.

The distribution of A_z for our sample of 80,000 SDSS galaxies is shown in Fig. 9. When calculating the probability distribution of A_z, we do not consider models with $r-i$ colours *redder* than the observed colour of the galaxy. This constrains $\mathrm{P}(A_z)$ to extend over positive values of A_z. The SDSS photometric errors are extremely small compared to the errors in the $\mathrm{D}_n(4000)$ and $\mathrm{H}\delta_A$ index. The main limiting factor in our analysis is the fact that we have used colours measured for the entire galaxy, but the spectra reflect the properties of the starlight that has found its way down a 3 arsecond diameter fibre that has been positioned close to the centre of the galaxy. Ideally we should use photometry that is matched to the fibre aperture to estimate the dust attenuation. This will only be available in a future release of the SDSS photometric pipeline (Lupton, private communication). The formal 2σ error on our estimate of A_z is typically around ± 0.1 mag.

Fig. 9 shows that the typical attenuation at z-band is quite small. The median value of A_z is 0.3 mag. Nevertheless there is a long tail to high values of A_z – more than 5% of galaxies in the sample are attenuated by more than a magnitude in the z-band. The dependences of A_z on absolute magnitude and on $\mathrm{D}_n(4000)$ are shown in Fig. 10. As can be seen, more luminous galaxies suffer more attenuation than less luminous galaxies. This agrees rather well with Wang & Heckman (1996) who have found that the dust opacity correlates strongly with galaxy luminosity. These authors derive an effective attenuation in the V-band that scales with luminosity as $\tau_V = 0.6(L_V/L_{V,*})^{0.5}$. This relation, converted to the z-band using our standard extinction curve, is shown as a red line on Fig 10. As can be seen, the agreement is very good at luminosities below L_*. At luminosities above L_* we derive lower attenuation values than Wang & Heckman (1996). This can be explained by the fact that their sample included only spiral galaxies, whereas our sample includes includes galaxies of all types. A substantial fraction of our high-luminosity objects are S0s and ellipticals. Fig. 10 also shows that galaxies with young stellar populations (small values of $\mathrm{D}_n(4000)$) are more attenuated by dust than galaxies with old stellar populations. This is expected because galaxies with young stars contain more gas and more dust than galaxies with old stellar populations.

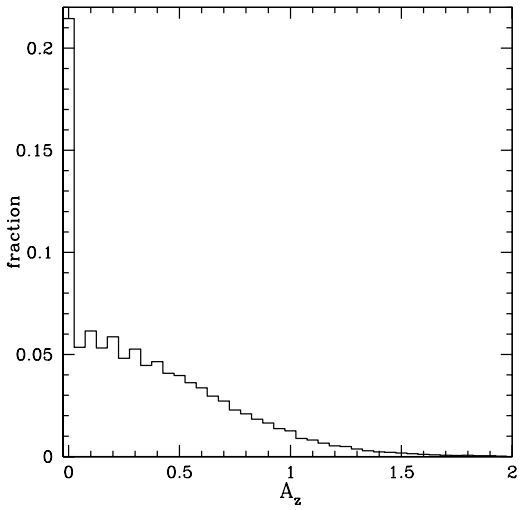

Figure 9: The distribution of the estimated values of the dust attenuation in the z-band for all the galaxies in the sample.

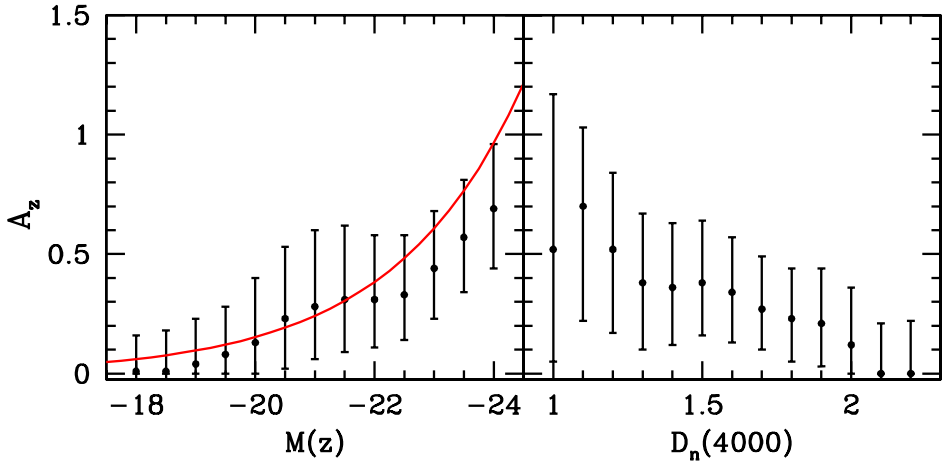

Figure 10: *Left:* A_z is plotted as a function of z-band absolute magnitude for all the galaxies in the sample. The red line shows the scaling relation of Wang & Heckman (1996) renormalized to the z-band. *Right:* A_z is plotted as a function of $D_n(4000)$. In both panels, the points indicate the median value of A_z and the error bars indicate the 25th to 75th percentiles of the distribution at a given magnitude.

5.4 Estimating Stellar Masses and Mass-to-Light Ratios

In this section, we present estimates of the the stellar masses and mass-to-light ratios of the galaxies in our sample. To estimate the stellar mass, we first need to estimate the dust-correction to the observed z-band magnitude of the galaxy, so we once again exclude models with $r - i$ colours redder than the observed colour. For each acceptable model, the stellar mass is computed by multiplying the dust-corrected luminosity of the galaxy by the stellar mass-to-light ratio predicted by the model. The best estimate of the mass is then obtained by weighting each model by the probability function in the usual way.

Our best estimates of the stellar mass divided by the observed z- band luminosity (i.e. luminosity *not* corrected for dust attenuation) of all 81,429 galaxies in the sample are plotted as a function of their z-band absolute magnitudes in the top panel of Fig. 11. The mass-to-light ratios are plotted in solar units, where we have adopted $M_{z\odot} = 4.48$ (Blanton et al. 2001). As can be seen, the distribution of $(M/L)_z$ is strongly dependent on galaxy luminosity. Almost all very luminous galaxies have high mass-to-light ratios. Faint galaxies span a wider range in $(M/L)_z$. For guidance, we have marked the value of $(M/L)_z$ for an unextincted galaxy that has formed stars at a constant rate over a Hubble time as a blue line on the plot. Galaxies with mass-to-light ratios lower than this value have had star formation histories that are more weighted towards the present than continuous star formation lasting 10-12 Gyr. Only a few of the most luminous galaxies fall into this category, but at faint magnitudes many galaxies have formed a large fraction of their stars at late times.

The bottom panel of Fig. 11 shows $(M/L)_z$ as a function of the standard concentration parameter C, defined as the ratio $R90/R50$, where R90 and R50 are the radii enclosing 90% and 50% of the Petrosian r-band luminosity of the galaxy. It has been shown by Shimasaku et al (2001) and Strateva et al (2001) that for bright galaxies, there is a good correspondence between concentration parameter and 'by-eye' classification into Hubble type, but there is some disgreement about the value of C that marks the boundary between early and late type galaxies. Strateva et al (2001) claim that galaxies with $C > 2.6$ are mostly early-type systems, whereas spirals and irregulars have $2 < C < 2.6$. Shimasaku et al (2001) recommend a $C = 3$ separator for an early-to-late cut at S0/Sa. Not surprisingly, our stellar mass-to-light ratios are also correlated with concentration parameter, with concentrated (early-type) galaxies exhibiting higher and more uniform values of $(M/L)_z$ than less concentrated (late-type) galaxies. In Fig. 11, the transition between these two regimes seems to occur at $C \sim 2.6$ in agreement with Strateva et al.

The distribution of errors on our stellar mass estimates is shown in Fig. 12. We plot the distribution of the 95% confidence range in $\log M_*$, i.e. the range of values of $\log M_*$ obtained when the 2.5% tails at each end of the probablity distribution of $\log M_*$ are excluded. For a Gaussian distribution of errors, this corresponds to four times the standard error in the mass estimate. As can be seen, the 95% confidence interval is typically around a factor ~ 2 in mass. The errors are smaller for older galaxies with larger 4000 Å breaks than for younger galaxies with smaller break strengths.

In Fig. 13, we plot the distribution of the stellar mass-to-light ratios of SDSS galaxies as a function of absolute magnitude in four of the five SDSS bands (g, r, i and z). We do not show results for the u-band because of difficulties with the K-corrections. The median value of the mass-to-light ratio in each absolute magnitude bin is shown as a solid symbol. Solid errorbars mark the 25th to 75th percentile ranges of the distributions. Dotted errorbars mark the 5th to 95th percentile ranges. As can be seen, the median mass-to-light ratio increases with luminosity in all pass bands. The scatter in M/L at fixed luminosity decreases at longer wavelengths: it is almost a factor of two larger in the g-band than in the z-band. In order to make some comparison to related work, we have plotted as a red line the mean relation between $(M/L)_r$ and r-band magnitude derived by Bernardi et al (2002) for a sample of early-type galaxies drawn from the SDSS. In this analysis $M/L \propto R_0\sigma^2/L$, where R_0 is the effective radius of the galaxy and σ is the line-of-sight velocity dispersion of the stars measured in a 3 arcsecond aperture. It is interesting that the relation derived by Bernardi et al agrees well with our M/L estimates at the highest luminosities but is somewhat high at lower values. This reflects the fact that our sample contains all types, and so is dominated by E/S0s only at the brightest magnitudes, whereas the Bernardi et al sample is carefully selected to contain only galaxies with pure, early-type spectra. Note that if we had assumed a Salpeter rather than a Kroupa (2001) IMF, our stellar mass estimates would have been more than a factor of two larger and would have been in clear contradiction with the dynamically-derived masses. However, it is also worth noting that the Bernardi et al dynamical mass estimates ignore contributions from rotational support and are estimated within a 3-dimensional effective radius, rather than the 2-dimensional projected half-light radius which is used to measure the light.

We note that the mass-to-light ratios of the most luminous galaxies in the survey appear to exhibit a great deal of scatter. Some of these galaxies have very large estimated dust attenuations, but 4000 Å break strengths that are typical of ordinary ellipticals. Others appear to have genuinely young stellar populations. We caution that our method of estimating stellar masses will break down if an AGN contributes significantly to the continuum emission shortwards of 4000 Å. A full investigation into the properties of the most luminous galaxies in the Universe is beyond the scope of this paper, but it is clear from this analysis that these objects are not very regular.

5.4.1 Aperture Effects

The $D_n(4000)$ and $H\delta_A$ indices measured from the SDSS spectra reflect the properties of the starlight that has found its way down a 3 arcsecond diameter fibre that has been positioned as close as possible to the centre of the galaxy. One may thus wonder to what extent our estimates of $(M/L)_z$ may be biased because the index measurements are not accurately reflecting the stellar content of the whole galaxy. In particular, aperture bias could well be a serious problem for spiral galaxies, where the index measurements may be appropriate for the central bulge component, but not for the outer disk where most of the star formation is taking place.

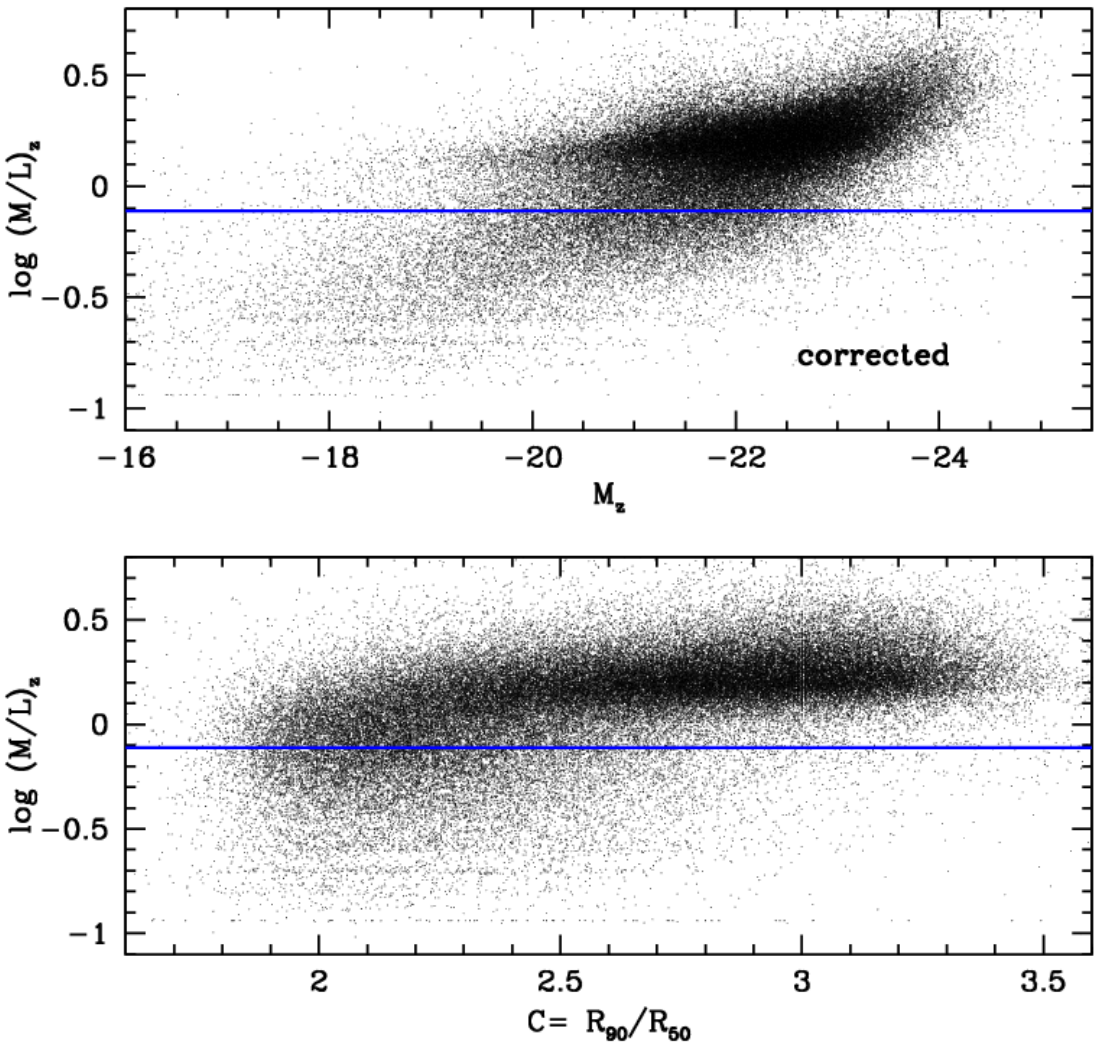

Figure 11: **Top:** $(M/L)_z$ is plotted as a function of z-band absolute magnitude for all galaxies in the sample. **Bottom:** $(M/L)_z$ is plotted as a function of r-band concentration parameter for all galaxies in the sample. The blue line indicates the value of $(M/L)_z$ for an unextincted galaxy that has been forming stars at a constant rate for a Hubble time.

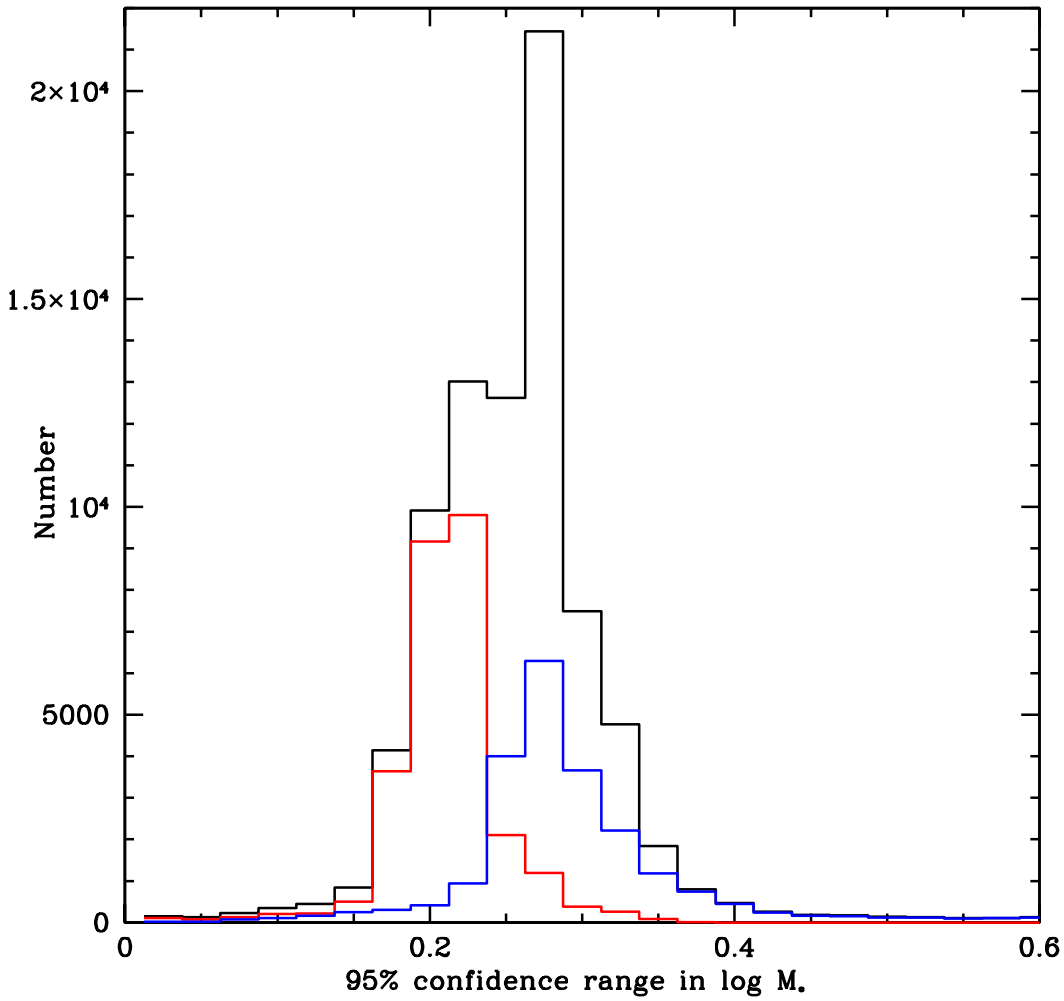

Figure 12: The distribution of errors in our stellar mass estimates. The quantity plotted is the full length of the 95% confidence interval in log M_*. The black histogram shows the distributions for all galaxies in the sample. The red histogram is for the subset of galaxies with $D_n(4000) > 1.8$ and the blue histogram is for galaxies with $D_n(4000) < 1.4$.

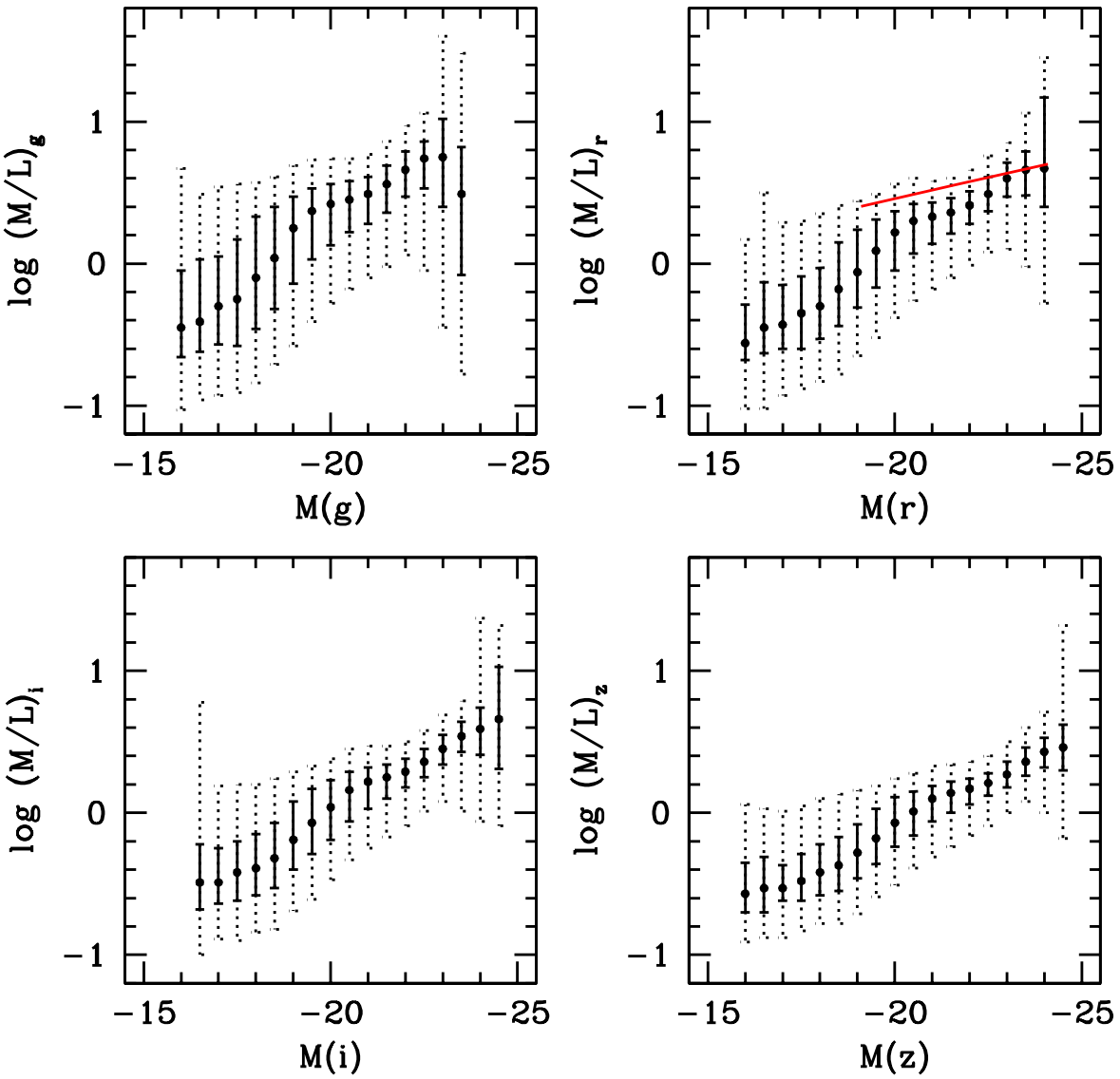

Figure 13: Mass-to-light ratios are plotted as a function of absolute magnitude in 4 SDSS bands. The solid symbols indicate the median mass-to-light ratio at a given magnitude, the solid errorbars indicate the 25th to 75th percentile ranges of the distribution and the dotted errorbars indicate the 5th-95th percentile ranges. Mass-to-light ratios are plotted in solar units where $M_{\odot g} = 5.07$, $M_{\odot r} = 4.62$, $M_{\odot i} = 4.52$ and $M_{\odot z} = 4.48$ (Blanton et al 2001). The red line is the mean relation between dynamical M/L (estimated from the stellar velocity dispersion) and r-band magnitude for a sample of early type galaxies from Bernardi et al (2002).

It is possible to address the effect of aperture bias in a statistical way by comparing the observed stellar indices and the derived M/L values for similar galaxies viewed at different distances from us. If aperture bias is important, one should see a trend in these quantities with distance.

This is illustrated in Figs. 14 and 15. We plot the index $D_n(4000)$ and the z-band mass-to-light ratio $(M/L)_z$ as a function of 'normalized' distance z/z_{max}, where z_{max} is the redshift at which the galaxy drops out of the survey. Normalizing by z_{max} takes care of any selection effects that arise when one divides up the sample in different ways. Note that as expected, galaxies in the survey are distributed uniformly in the quantitity $V/V_{max} = (z/z_{max})^3$, so there are many more objects in the bins with z/z_{max} values close to 1.

Fig. 14 shows the variation in the 4000 Å break as a function of normalized distance. We see that both the size and the sense of the effect depend strongly on the absolute magnitude of the galaxy. Galaxies with luminosities $\sim L_*$ ($M_*(z) = -22.3$) exhibit the strongest trend with z/z_{max}. More distant galaxies have younger stellar populations than nearby objects, as expected if the spectra are preferentially sampling the bulges of nearby galaxies.

Fig. 15 shows the trend in our estimates of $(M/L)_z$ with distance. As can be seen, these remain constant or even rise with increasing z/z_{maz}. How can this be understood? As we have shown in Fig. 14, the models will overestimate the mean stellar ages of nearby L_* galaxies and this should lead to M/L values that decrease as a function of z/z_{max}. However, the models will also underestimate the amount of dust attenuation in the nearby systems (recall that this is estimated by comparing the colour of the best-fit model with the colour of the galaxy as a whole). These two effects tend to cancel each other out. In the brightest galaxies, the effect due to dust dominates and the most distant galaxies have slightly *higher* estimated mass-to-light ratios on average than the nearby ones.

Unfortunately it is not possible use the relations shown in Figs. 14 and 15 to estimate the true global mass-to-light ratio of a given type of galaxy. Even at the outer limit of the survey, the median fraction of the total galaxy light that enters the fiber is around 50%. A sample of galaxies with large aperture spectra is required for this purpose. Nevertheless, our plots make it clear that the variations in M/L as a function of luminosity and concentration shown in Figs. 11 and 13 are substantially larger than any biases induced by aperture effects.

5.4.2 Comparison with Colour-Based Methods

Most previous attempts to convert from absolute magnitude to stellar mass have used colours to constrain the star formation histories of galaxies (e.g. Brinchmann & Ellis 2000; Cole et al 2001; Bell & de Jong 2001), Bell & de Jong (2001) argue that there should be a tight relation between the optical colours of spiral galaxies and their stellar mass-to-light ratios. This relation ought to be insensitive to the effects of dust-reddening. Although dust causes colours to become redder, it also makes the galaxy fainter and for a standard dust attenuation curve, the two effects compensate. Bell & de Jong (2001) show that recent bursts of star formation introduce scatter into this relation, but claim that this should not be important for most

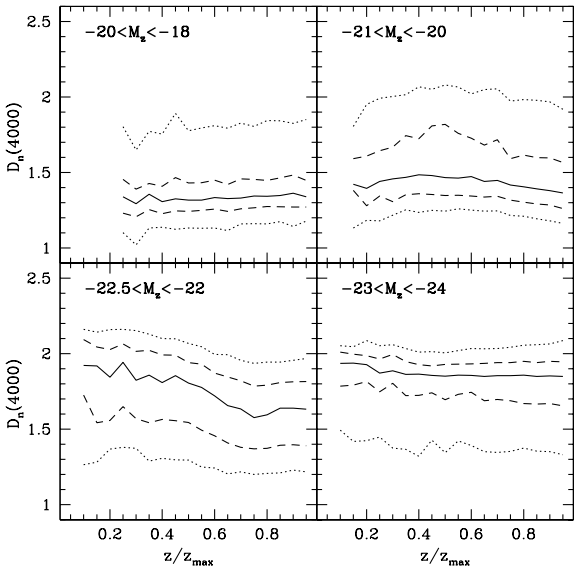

Figure 14: The $D_n(4000)$ index is plotted as a function of z/z_{max} for galaxies in different ranges of z-band absolute magnitude. The solid line indicates the median of the distribution as a function of z/z_{max}. The dashed lines indicate the 25th and 75th percentiles. The dotted lines indicate the 5th and 95th percentiles.

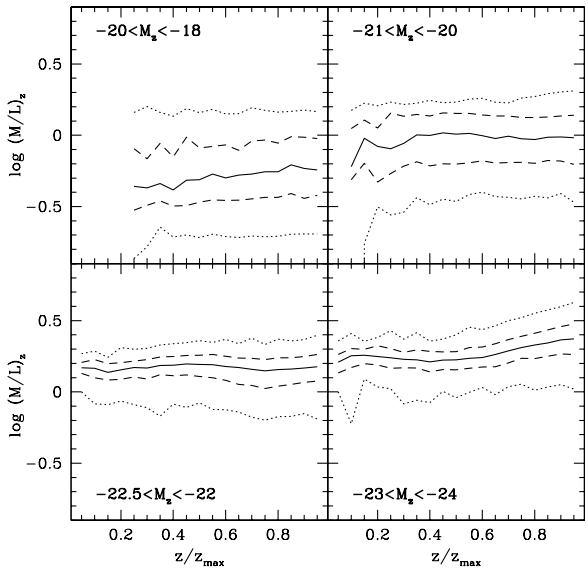

Figure 15: The stellar mass-to-light ratio in the z-band is plotted as a function of z/z_{max} for galaxies in different ranges of z-band absolute magnitude.

spirals in Tully-Fisher samples.

It is interesting to see whether the stellar masses derived using our method do correlate with the observed optical colours of galaxies as predicted by Bell & de Jong. In Fig. 16 we plot the stellar mass-to-light ratio in the g-band as a function of the K-corrected $g-r$ colour for galaxies in 4 different absolute magnitude ranges. At luminosities $\sim L*$, we find that there is a tight relation between colour and stellar mass-to-light ratio, as predicted. However, for fainter galaxies, the relation breaks down quite badly. For galaxies with $M_z > -21$, there is a scatter of more than a factor of three in mass-to-light ratio for galaxies with $g-r < 0.3$. For galaxies with $M_z > -20$, there is a large scatter in M/L for galaxies of all colours.

We note that in their analysis, Bell & de Jong only consider exponential star formation histories with ages of 12 Gyr. We find that a substantial fraction of galaxies with luminosities less than $\sim L_*$ have mean stellar ages that are considerably younger than predicted if stars form at a constant rate for a Hubble time (see Fig. 11). Moreover, as we will show in detail in Paper II, a large fraction of sub-L_* galaxies have experienced recent bursts.

The results of our comparison show that although colours may be a good way of constraining the stellar mass-to-light ratios of luminous spiral galaxies at the present day, they should not be used for fainter objects. It might also be dangerous to apply such methods to high redshift galaxies, which are by definition younger and may be forming a larger fraction of their stars in bursts (Somerville, Primack & Faber 2001).

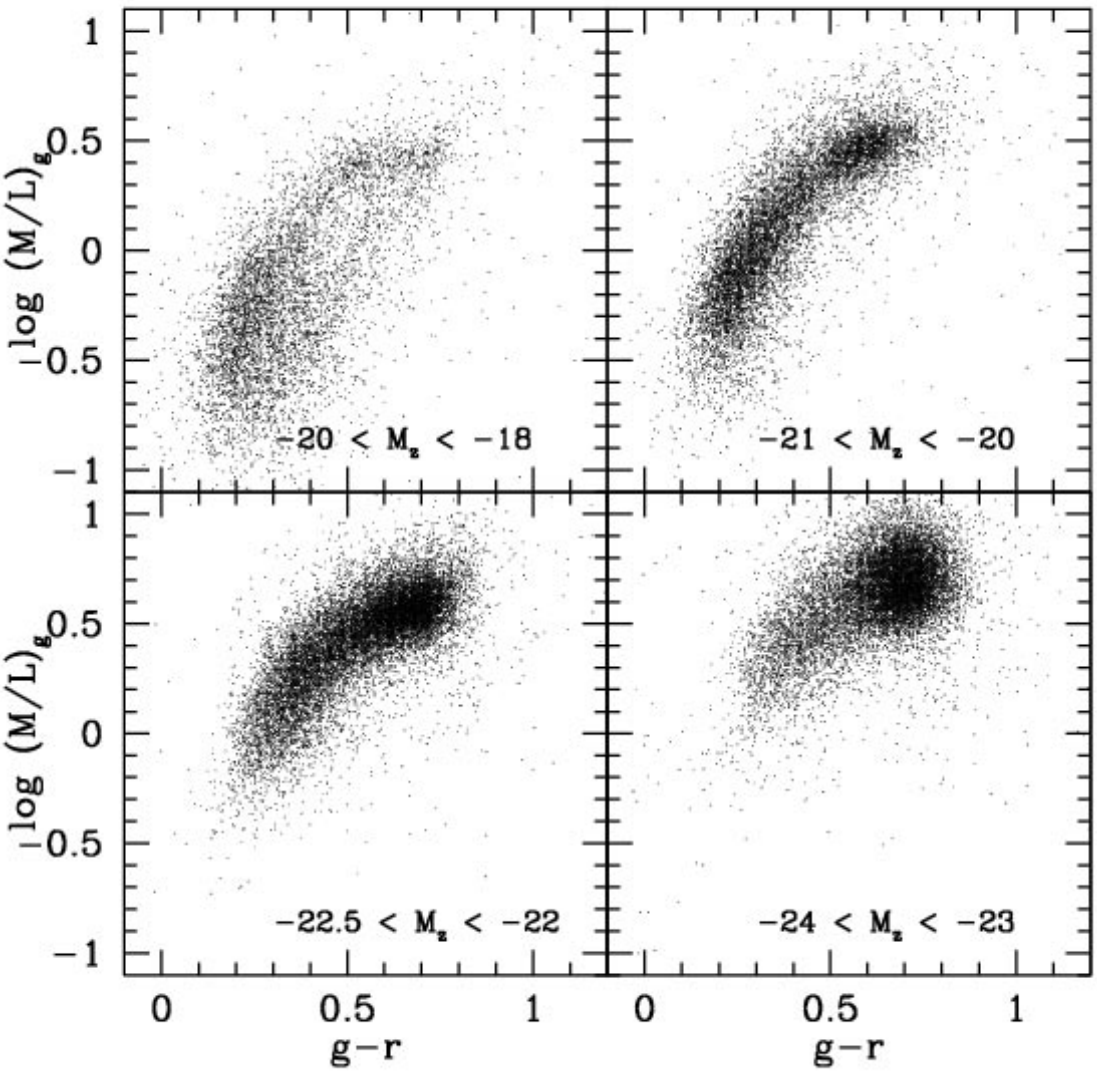

Figure 16: The g-band mass -to-light ratio is plotted as a function of K-corrected $g-r$ colour for galaxies in 4 different bins of z-band absolute magnitude.

6 An Inventory of the Stellar Mass in the Universe

In this section, we compute how galaxies of different types contribute to the total stellar mass budget of the local Universe. Galaxies of different luminosities can be seen to different distances before dropping out due to the selection limits of the survey. The volume V_{max} within which a galaxy can be seen and will be included in the sample goes as the distance limit cubed, which results in galaxy samples being dominated by intrinsically bright galaxies. In this paper we use the simplest method available for correcting for selection effects, the V_{max} correction method (Schmidt 1968). Each galaxy is given a weight equal to the inverse of its maximum visibility volume determined from the apparent magnitude limit of the survey. In order to obtain an estimate of the true number density of galaxies in the Universe, it is necessary to account for galaxies that are missed due to fibre collisions or spectroscopic failures. This affects around 10-15% of the galaxies brighter than the spectroscopic limit of the survey (Blanton et al 2001). Here, we focus on the *relative* contribution of different kinds of galaxies to the total stellar mass, so weighting by $1/V_{max}$ ought to be sufficient. As a check, we have computed the z-band luminosity function for the galaxies in our sample and find that the Schechter function fit given in Blanton et al (2001) provides an excellent match to the shape of the function we derive.

A compendium of results is presented in Fig. 17. We plot the fraction of the total stellar mass contained in galaxies as a function of their stellar mass, $\mathrm{D}_n(4000)$, $g-r$ colour, F_{burst}, size, concentration index and surface mass density. Note that we have adopted a cosmology with $\Omega = 0.3$, $\Lambda = 0.7$ and $\mathrm{H}_0 = 70$ km s^{-1} Mpc^{-1} in our calculations. From these plots it is possible to read off the characteristic properties of the galaxies that contain the bulk of the stellar mass in the Universe at the present day. Note that because we have more than 80,000 galaxies in the total sample, we are able to derive extremely accurate functional forms for these distributions. The bins around the peaks of the distributions shown in Fig. 17 each contain 5000 or more galaxies. Even in the wings, most bins are still sampled by a few hundred objects. In Table 1, we list the median, 1%, 5%, 25%, 75%, 95% and 99% percentile values for each of the distributions shown in Fig. 17 (with the exception of F_{burst}).

Our main conclusions are the following:

- The characteristic mass M_{char} of galaxies at the present day, defined as the peak of the distribution function shown in the top left panel of Fig. 17, is $7 \times 10^{10} M_{\odot}$. This agrees reasonably well with the results of Cole et al. (2001). These authors transform the near-infrared luminosity function derived from 2dF/2MASS data to a stellar mass function using a colour-based technique. Their Schechter-function parametrization yields $M_{char} = 5.6 \times 10^{10} M_{\odot}$ for $\mathrm{H}_0 = 70$ km s^{-1} Mpc^{-1} and a Kennicutt (1983) IMF, which is fairly close to the Kroupa (2001) IMF that we have assumed.

  We find that only 15% of the total stellar mass is contained in galaxies less massive than $10^{10} M_{\odot}$. An even smaller fraction ($\sim$3%) of the total mass in contained in galaxies less massive than $10^{9} M_{\odot}$. The total stellar mass budget of the Universe is thus heavily weighted towards galaxies that are within a factor of 10 in mass of our own Milky Way.

- The $D_n(4000)$ distribution of the stellar mass is strongly bimodal. The first peak is centred at $D_n(4000) \sim 1.3$. Galaxies with break strengths of this value have r-band weighted mean stellar ages of $\sim 1-3$ Gyr and mass-weighted mean ages a factor ~ 2 larger. Almost all these galaxies also have emission lines and are thus forming stars at the present day. The second peak is centred at $D_n(4000) \sim 1.9$, a value typical of old elliptical galaxies with mean stellar ages ~ 10 Gyr.

- The $g-r$ colour distribution of the stellar mass shows the same bimodality as the $D_n(4000)$ distribution, except that the "blue" peak is less pronounced. This is probably because colours depend both on stellar age and on dust attenuation, whereas $D_n(4000)$ is not affected by dust. Note that Strateva et al (2001) have also discussed the bimodality in the colour distributions of SDSS galaxies.

- At least 95% of the total stellar mass is located in galaxies that have *not* experienced a burst in the past 2 Gyr. Note that the confidence intervals on the burst mass fractions are broad and generally skewed towards low values of F_{burst} – this is why we say 'at least'.

- The distribution of stellar mass as a function of galaxy half-light radius in the r-band (R_{50}) is peaked at ~ 3.5 kpc. For the radius containing 90% of the light (R_{90}) it is peaked at ~ 9 kpc. More than 90% of the total stellar mass in the Universe resides in galaxies with R_{50} and R_{90} that are within a factor three of these values.

- The distribution of stellar mass as a function of concentration index is broad, with no pronounced peak at any particular value. If we adopt $C = 2.6$ as the demarcation between early and late-type galaxies, then 61% of the total stellar mass is contained in the early-types. If we adopt $C = 3$, then only 15% of the mass is contained in such systems.

- We define the surface mass density μ_* as $0.5M_*/(\pi z_{50}^2)$, where z_{50} is the Petrosian half-light radius in the z-band. Most of the stellar mass in the Universe resides in galaxies with μ_* within a factor of 2 of $10^9 M_\odot$ kpc^{-2}.

Table 1: Percentiles of the distribution of the fraction of the total stellar mass contained in galaxies of different types shown in Fig. 17

Parameter	Median	1%	5%	25%	75%	95%	99%
$\log M_*$ ($M_\odot$)	10.667	8.606	9.408	10.267	11.043	11.598	11.897
$D_n(4000)$	1.684	1.110	1.214	1.425	1.851	2.002	2.101
$g-r$	0.566	0.112	0.231	0.424	0.654	0.750	0.820
R_{50} (kpc)	3.860	0.247	0.964	2.524	5.524	9.030	12.832
R_{90} (kpc)	10.591	1.631	3.446	7.042	15.345	26.696	38.950
$C = R_{90}/R_{50}$	2.614	1.788	1.947	2.312	2.879	3.161	3.317
$\log \mu_*$ ($M_\odot$ kpc^{-2})	8.808	7.288	7.859	8.521	9.009	9.317	9.661

7 Summary and Discussion

We have developed a new method to constrain the past star formation histories of galaxies. It is based on two stellar absorption line indices, the 4000 Å break strength $D_n(4000)$ and the Balmer absorption line index $H\delta_A$. Together these two indices allow us to place constraints on the mean age of the stellar population of a galaxy and the fraction of its stellar mass formed in recent bursts.

We have generated a library of Monte Carlo realizations of different star formation histories, which includes bursting as well as continuous models and a wide range of metallicities. We use the library to generate estimates and confidence intervals for a variety of parameters for a sample of 80,000 galaxies drawn from the Sloan Digital Sky Survey, These include:

1. F_{burst} the fraction of the stellar mass of the galaxy formed in bursts in the past two Gyr.
2. A_z the attenuation of the rest-frame z-band light due to dust.
3. Stellar mass-to-light ratios in the g, r, i and z bands.
4. Stellar masses.

Note that the analysis can be extended to include other parameters describing the star formation history of a galaxy. Not all parameters are equally well-constrained. For example, the luminosity-weighted or mass-weighted mean stellar ages have large errors, because of the rather strong dependence of the 4000 Å break on metallicity at ages of more than 1-2 Gyr (see Fig. 1).

In the first part of the paper, we have illustrated in detail how our methods can be applied to galaxies in the SDSS and we have estimated the confidence with which we can constrain

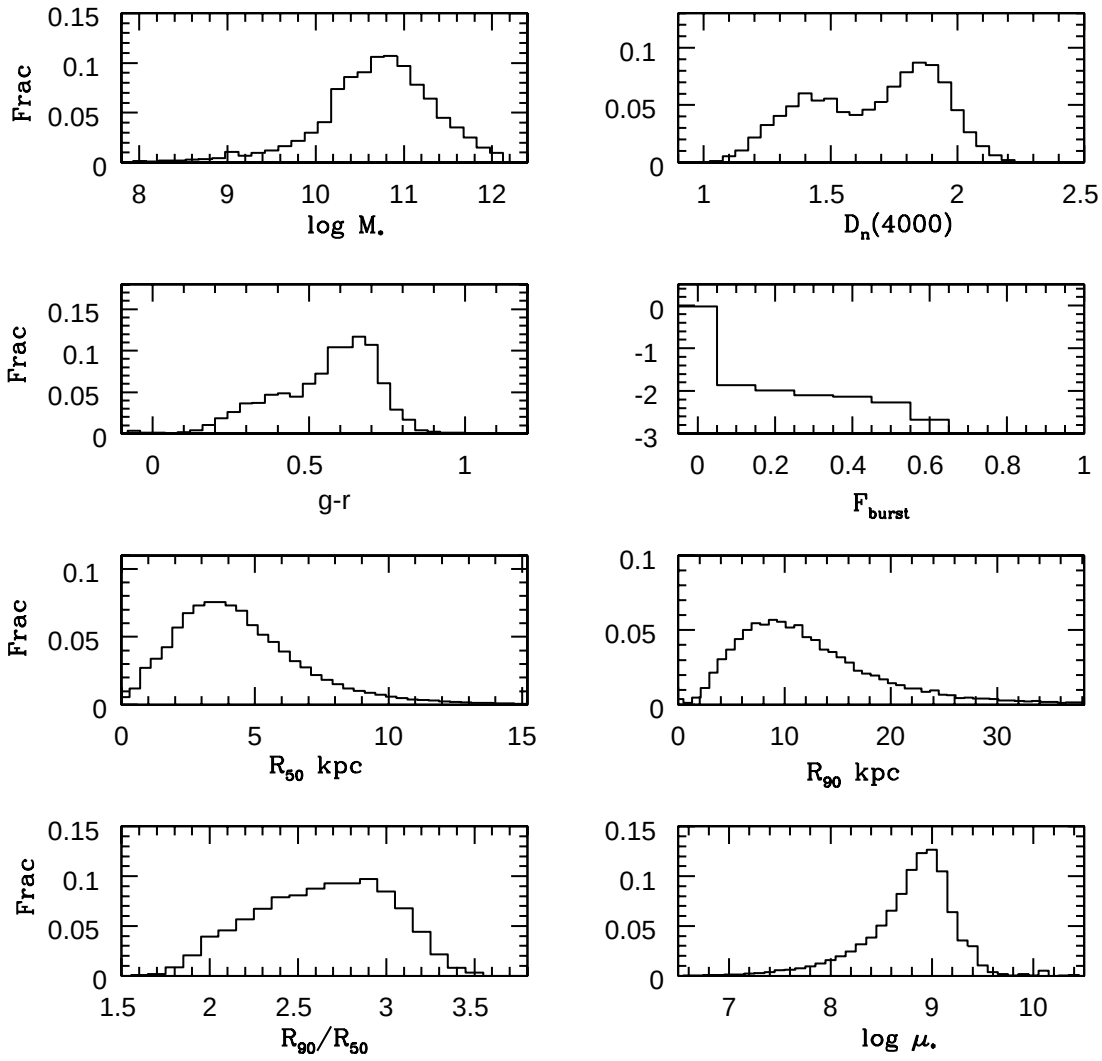

Figure 17: The fraction of the total stellar mass in the Universe contained in galaxies as a function of 1) log stellar mass, 2) $D_n(4000)$, 3) $g-r$ colour K-corrected to z=0, 4) F_{burst}, 5) Petrosian half-light radius in the r-band, 6) Petrosian 90% radius on the r-band, 7) concentration index (R_{90}/R_{50}), 8) log surface mass density. The fraction is shown linearly in all plots except that for F_{burst} where the logarithm is given.

basic parameters such as stellar masses. In the second part of the paper, we have presented a number of astrophysically interesting applications of our methods.

We have shown that the attenuation of the z-band light due to dust depends strongly on both the absolute magnitude and the mean stellar age of a galaxy. We have also studied the distribution of stellar mass-to-light ratios of galaxies as a function of absolute magnitude in the four SDSS pass bands. We have shown that the distribution of M/L is strongly dependent on galaxy luminosity in all photometric bands. Almost all very luminous galaxies have high mass-to-light ratios. Faint galaxies have lower mass-to-light ratios, but also span a wider range in M/L. We have also shown that the scatter in M/L at a given luminosity is a factor of ~ 2 smaller in the z-band than it is in the g-band. Finally, we have computed how galaxies of different types contribute to the total stellar mass budget of the Universe.

In the standard paradigm for structure formation in the Universe, galaxy formation occurs hierarchically through the merging of small protogalactic condensations to form more and more massive systems. In this picture, the contribution of different kinds of galaxies to the stellar mass budget is expected to evolve strongly with redshift. The rate and form of this evolution depend not only on the values of cosmological parameters such as Ω and Λ, but also on the physical processes that control the rate at which stars form in galaxies. For example, if star formation rates are enhanced during galaxy-galaxy mergers, the fraction of stars formed in recent bursts should rise strongly with redshift, simply because merging rates and gas fractions were higher in the past (see for example Kauffmann & Haehnelt 2000).

Although it is now clear that the integrated star formation rate density increases strongly to higher redshifts (Madau et al 1996), it is still not understood which galaxies undergo the strongest evolution or which physical processes cause galaxies to form stars more rapidly in the past. In the next few years, there will be a number of new large redshift surveys of the faint galaxy population. These surveys will contain enough galaxies to carry out an inventory of the stellar mass at $z \sim 1$. When these results are compared with the distributions derived from the SDSS, it will be possible to draw quantitative conclusions about how galaxies have evolved over past two thirds of a Hubble time and to begin disentangling the effects of the different processes that may have influenced this evolution.

S.C. thanks the Alexander von Humboldt Foundation, the Federal Ministry of Education and Research, and the Programme for Investment in the Future (ZIP) of the German Government for their support.

The Sloan Digital Sky Survey (SDSS) is a joint project of The University of Chicago, Fermilab, the Institute for Advanced Study, the Japan Participation Group, The Johns Hopkins University, Los Alamos National Laboratory, the Max-Planck-Institute for Astronomy (MPIA), the Max-Planck-Institute for Astrophysics (MPA), New Mexico State University, Princeton University, the United States Naval Observatory, and the University of Washington. Apache Point Observatory, site of the SDSS telescopes, is operated by the Astrophysical Research Consortium (ARC).

Funding for the project has been provided by the Alfred P. Sloan Foundation, the SDSS member institutions, the National Aeronautics and Space Administration, the National Science Foundation, the U.S. Department of Energy, the Japanese Monbukagakusho, and the Max Planck Society. The SDSS Web site is http://www.sdss.org/.

Appendix A

Here we describe the mathematical and statistical underpinning of the Bayesian likelihood estimates for parameters such as F_{burst}, A_z and M/L that we derive in this paper.

Let us recall the basis of Bayesian statistics for this kind of problem. An initial assumption is made that the data are randomly drawn from a distribution which is a member of a model family characterised by a parameter vector $\mathbf{P}$. The dimension of $\mathbf{P}$ can, in principle, be arbitrarily large. In particular, it can be much larger than the number of points N in the dataset to be fitted. The goal is then to use the data to define a likelihood function on the space of all possible $\mathbf{P}$. This function can be used to obtain a best estimate and confidence interval for any model property Y($\mathbf{P}$).

In Bayesian statistics one has to specify a prior distribution on the space of all possible $\mathbf{P}$. This is a probability density distribution $f_p(\mathbf{P})$ which encodes knowledge about the relative likelihood of various $\mathbf{P}$ values in the absence of any data. For example, the physically accessible range for each element of $\mathbf{P}$ may be limited. Typically one takes a uniform prior in parameters with a small dynamic range and a uniform prior in the log of parameters with a large dynamic range.

The likelihood of a particular value of $\mathbf{P}$ given a specific dataset $\mathbf{d}$ is then written as a posterior probability density function (using Bayes' theorem) as

$$f(\mathbf{P} \mid \mathbf{d})d\mathbf{P} = Af_p(\mathbf{P})Pr\{\mathbf{d} \mid \mathbf{P}\}d\mathbf{P} \tag{2}$$

where A is a constant which is adjusted so that $f(\mathbf{P} \mid \mathbf{d})$ normalises correctly to unity and $Pr\{\mathbf{d} \mid \mathbf{P}\}$ is the probability of the observed dataset on the hypothesis that the underlying distribution is described by the particular parameter set $\mathbf{P}$.

The likelihood of the derived parameter Y($\mathbf{P}$) given the data is then

$$f(Y \mid \mathbf{d})dY = \int_Y f(\mathbf{P} \mid \mathbf{d})d\mathbf{P} \tag{3}$$

where the integral extends over all $\mathbf{P}$ for which Y lies in a specified bin $\pm$dY/2. Note that there is no regularity requirement on the function Y($\mathbf{P}$) other than piecewise continuity so it makes sense to define a probability density. The most likely value of Y can then be taken as the peak of this distribution; the most typical value as its median; the 95% (symmetric) confidence interval for scalar Y can be defined by excluding the 2.5% tails at each end of the distribution.

When applied to the kinds of problems presented in this paper, the prior is taken to be the distribution of possible star formation histories in the comparison library, which can be viewed as a Monte Carlo sampling of $f_p(\mathbf{P})$. The integral in the above expression for the likelihood of Y is then trivially evaluated through binning the integrand as a function of Y. The expression for $Pr\{\mathbf{d} \mid \mathbf{P}\}$ is also straightforward for our case, since we have a measure of each element of $\mathbf{d}$ and we can assume the errors are normal with known correlation matrix C. In this situation

$$Pr\{\mathbf{d} \mid \mathbf{P}\} \propto \exp[-(\mathbf{d} - \mathbf{d}_p(\mathbf{P})).\mathrm{C}^{-1}.(\mathbf{d} - \mathbf{d}_p(\mathbf{P}))/2] \tag{4}$$

where $\mathbf{d}_p(\mathbf{P})$ is the data vector predicted by the model with parameters $\mathbf{P}$. The argument of the exponential is then just minus one half of χ^2.

It is worth noting that this procedure makes no assumptions about the shapes of the distributions $f_p(\mathbf{P})$, $f(\mathbf{P} \mid \mathbf{d})$ or $f(Y \mid \mathbf{d})$. The first can be assumed at will, and for small error bars and a well constrained problem should have little effect on the answer. The other two are then derived consistently. The important assumptions are that the model makes a well defined and specific prediction for the value of the observable in the absence of observational errors (in practice there will be some degree of theoretical uncertainty and this could be included in C if it can be modelled as Gaussian) and that the observed data $\mathbf{d}$ have a known observational error which can be assumed Gaussian with covariance matrix C.

References

Balogh, M.L., Morris, S.L., Yee, H.K.C., Carlberg, R.G., Ellingson, E., 1999, ApJ, 527, 54

Bell, E.F., De Jong, R., 2001, ApJ, 550, 212

Bernardi, M., Sheth, R.K., Annis, J., Burles, S., Eisenstein, D.J., Finkbeiner, D.P., Hogg, D.W., Lupton, R.H., Schlegel, D.J., SubbaRao, M. et al., 2002, AJ, submitted (astro-ph/0110344)

Blanton, M.R., Dalcanton, J., Eisenstein, D., Loveday, J., Strauss, M.A., SubbaRao, M., Weinberg, D.H., Andersen, J.E. et al., 2001, AJ, 121, 2358

Brinchmann, J., Ellis, R.S., 2001, ApJ, 536, L77

Bruzual, A.G., 1983, ApJ, 273, 105

Bruzual, A.G., Charlot, S., 1993, ApJ, 405, 538

Calzetti, D., Kinney, A., Storchi-Bergmann, T., 1994, ApJ, 429, 582

Charlot, S., Fall, S.M., 2000, ApJ, 539, 718

Cole, S., Norberg, P., Baugh, C.M., Frenk, C.S., Bland-Hawthorn, J., Bridges, T., Cannon, R., Colless, M. et al, 2001, MNRAS, 326, 255

Ferreras, I., Charlot, S., Silk, J., 1999, ApJ, 521, 81

Fukugita, M., Ichikawa, T., Gunn, J.E., Doi, M., Shimasaku, K., Schneider, D.P., 1996, AJ, 111, 1748

Gunn, J.E., Carr, M., Rockosi, C., Sekiguchi, M., Berry, K., Elms, B., de Haas, E., Ivezic, Z. et al, 1998, AJ, 116, 3040

Hogg, D.W., Finkbeiner, D.P., Schlegel, D.J., Gunn, J.E., 2001, AJ, 122, 2129

Kauffmann G., Haehnelt M., 2000, MNRAS, 311, 576

Kauffmann, G. et al. 2002, in preparation (Paper II)

Kennicutt, R.C., 1983, ApJ, 272, 54

Kroupa, P., 2001, MNRAS, 322, 231

Lupton, R.H. et al, 2002, in preparation

Madau, P., Ferguson, H.C., Dickinson, M.E., Giavalisco, M., Steidel, C.C., Fruchter, A., 1996, MNRAS, 283, 1388

McKay, T.A., Sheldon, E.S., Racusin, J., Fischer, P., Seljak, U., Stebbins, A., Johnston, D.,

Frieman, J.A. et al., 2002, ApJ, submitted (astro-ph/0108013)

Schlegel, D.J., Finkbeiner, D.P., Davis., M., 1998, ApJ, 500, 525

Shimasaku, K., Fukugita, M., Doi, M., Hamabe, M., Ichikawa, T., Okamura, S., Sekiguchi, M., Yasuda, N. et al, 2001, AJ, 122, 1238

Schmidt, M., 1968, ApJ, 151, 393

Smith, J.A., Tucker, D.L., Kent, S., Richmond, M.W., Fukugita, M., Ichikawa, T., Ichikawa, S.I.,Jorgensen, A.M. et al. 2002, AJ, in press

Somerville, R.S., Primack, J.R., Faber, S.M., 2001, MNRAS, 320, 504

Stoughton, C., Lupton, R.H., Bernardi, M., Blanton, M.R., Burles, S., Castander, F.J., Connolly, A.J., Eisenstein, D.J. et al., 2002, AJ, 123, 485

Strateva, I., Ivezic, Z., Knapp, G.R., Narayanan, V.K., Strauss, M.A., Gunn, J.E., Lupton, R.H., Schlegel, D. et al, 2001, AJ, 122, 1861

Strauss, M.A. et al, 2002, AJ, submitted

Tremonti, C.A. et al., 2002, in preparation

Verheijen, M.A.W., 2001, ApJ, 563, 694

Wang, B., Heckman, T.M., 1996, ApJ, 457, 645

Worthey, G., 1994, ApJS, 95, 107

Worthey, G., Ottaviani, D.L, 1997, ApJS, 111, 377

York D.G., Adelman J., Anderson J.E., Anderson S.F., Annis J., Bahcall N.A., Bakken J.A., Barkhouser R. et al., 2000, AJ, 120, 1579

Zaritsky, D., Smith, R., Frenk, C.S., White, S.D.M., 1993, ApJ, 405, 464